

MECHANICAL TESTING OF DEPLOYABLE THIN SHELL CFRP BOOMS IN IDEAL AND  
REALISTIC INTERFACES FOR THE SOLAR SAIL DEMONSTRATOR GOSSAMER-1  
**27-30 September 2016, Toulouse, France**

**Martin E. Zander**<sup>(1)(2)</sup>, **Andreas Wilken**<sup>(2)</sup>, **Michael Sinapius**<sup>(1)</sup>, **Christian Hühne**<sup>(2)</sup>

<sup>(1)</sup> *Institute of Adaptronics and Function Integration (IAF), Technische Universität Braunschweig,  
Langer Kamp 6, 38106 Braunschweig, Germany  
Email: martin.zander@tu-braunschweig.de*

<sup>(2)</sup> *Institute of Composite Structures and Adaptive Systems (DLR-FA), Deutsches Zentrum für Luft-  
und Raumfahrt e.V. (DLR), Lilienthalplatz 7, 38108 Braunschweig, Germany  
Email: martin.zander@dlr.de*

## **ABSTRACT**

Gossamer space structures like solar sails, drag sails or solar arrays expand to very large dimensions while at the same time aiming for low masses, leading to a low areal density. In many cases these applications are designed using long lightweight booms, spanning out sails or other membranes. For launch and transfer however the booms need to be stowable and compact, while they are demanded to withstand the sail loads during deployment and in operation phase. In DLR's Solar Sail demonstrator Gossamer-1, a 5 m x 5 m squared solar sail, four sail quadrants are spanned out by four thin shell CFRP booms. Facilitating a tip deployment, the booms are flattened and coiled each on a cylinder of a deployment unit for stowage, while the boom roots are fixed in an interface to the spacecraft bus in a cross like arrangement. Having its purpose in transferring occurring boom loads into the main structure, the interface needs to be flexible at the same time, mimicking the changing cross section of the boom, once it deploys and transforms from flat to its full cross sectional dimensions. Another interface connects the sails to the booms, while holding the boom's cross section in a semi-deployed state. These found conditions are imperfect compared to using the full cross sectional shape of the boom with its full second moment of area and an ideally clamped root fixation. Simulating the boom and its interfaces of the Gossamer-1 demonstrator, several booms are tested in an advanced vertical boom test stand at the DLR Space Structures Lab @ Uni of DLR Braunschweig. Mechanical characteristics and properties of full scale booms with ideal boundary conditions and realistic interfaces are being investigated, enabling a direct comparison. Applying certain realistic load cases, like lateral bending, axial compression and combinations of both, thresholds and robustness as well as load carrying capabilities after buckling several times are quantified in practical tests. Thus characterizing the Gossamer-1 boom under ideal and realistic boundary conditions is realized, specifying the boom performance in reality and providing the base for a robust Gossamer Spacecraft design that facilitates thin shell CFRP booms. This paper gives a detailed insight on the test stand and setup, used interfaces and boundary conditions, testing procedures, and discusses the test results of both configurations on characteristic load-displacement curves and acquired values for buckling failure design.

## **1. INTRODUCTION**

Solar sailing is seen as a future alternative propulsion technology, using accumulated impulses of photons from the solar wind. Such solar sail applications are found in the class of so called Gossamer structures. Generally such structures provide large areas or large volumes at low mass demanding a delicate and expandable supporting structure.

Gossamer-1 (Gos-1) is a 5.3 m x 5.3 m, rigid, squared solar sail demonstrator, with the main focus on showing its ability to deploy its four booms and four sails on a low earth orbit in a controlled manner, as well as the successful use of thin film photovoltaic and proving overall system qualification. As the trailblazer mission Gos-1 is the first of three steps of the “Gossamer Roadmap” of DLR and ESA [1], developed in 2009. It is a scaled down version of a fully functional solar sail, without the necessity of using attitude and orbit control or navigation. The “Gossamer Roadmap” aimed for ultra-lightweight deployable technology that is scalable in size and complexity and applicable for thin film space structures, in specific solar sailing technology, solar power generation and de-orbiting. In general this multistep strategy aimed for the application and augmentation Gossamer technology of DLR in terms of CFRP boom & deployment mechanism technology, thin foil technology and space system competence. Although the “Gossamer Roadmap” is not pursued in its original extend, scalable ultra-lightweight and deployable technology for other than solar sail applications is still in the focus of research at DLR.

The main components of Gos-1 are the central spacecraft unit, the main structure, hosting the electronic and communication system, and two crossing light weight CFRP booms, each of 8 m in length, that span out the four sail quadrants. Deployment of booms and sails is simultaneously realized by four remotely controlled deployment units that are unrolling the stowed booms from their hubs with electric motors. Once the sails and booms have reached their full expansion, the deployment units separate and are floating away, as further described in [2]. Displaying the main components and main dimensions in Fig. 1, the deployment process can be followed in the image as well.

Apart from experiencing launch loads and present space environment in LEO, such as large temperature gradients, low pressure, atomic oxygen, radiation, and resulting effects like creep [3], mechanical loads on booms and sails that occur during deployment and in flight configuration can generate prevalent risks. Thus to reduce these and to secure mission success, investigations on the mechanical behavior under load of the used thin shell CFRP booms were performed and are presented in this paper.

Characterizing the booms mechanically and their buckling behavior, threshold loads for lateral bending and axial loading were acquired for two different boom interfaces. A clamping device maintaining the full cross sectional area of the boom, representing an ideal fixation at the boom root, and a realistic, flexible, boom-spacecraft-interface were used to simulate the boom connection to the spacecraft. Latter interface type enables the boom to reduce its cross sectional dimensions necessary for stowage, when the boom is flattened and rolled up, and changing its cross section throughout the deployment process. The loading is simulated using a recently introduced vertical test stand determining critical buckling loads and load carrying capabilities.

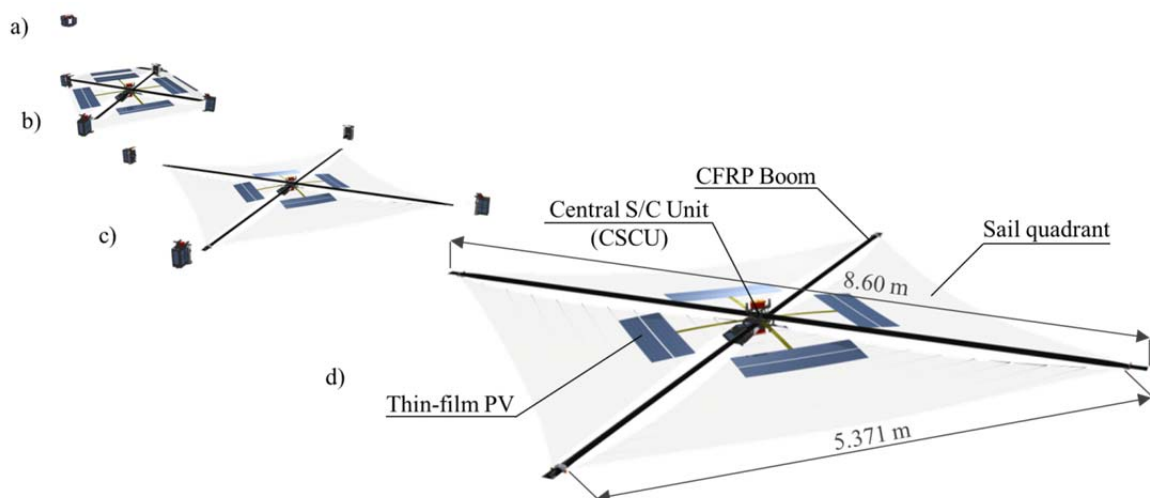


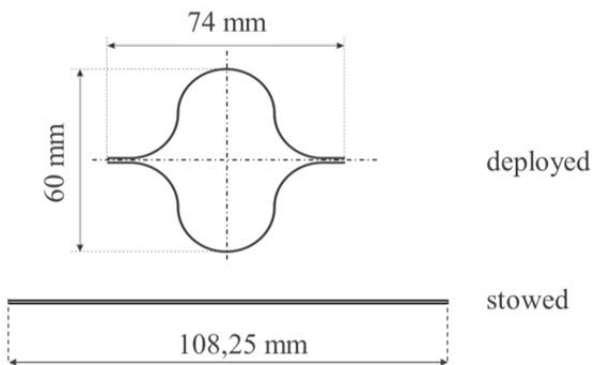
Fig. 1: Deploying Gossamer-1 spacecraft with main components and main dimensions; a) Gossamer-1 stowed, b) deployment in progress, c) fully deployed & jettisoning of deployment units, d) fully deployed Gossamer-1

## 2. BOOM & INTERFACE ARCHITECTURE

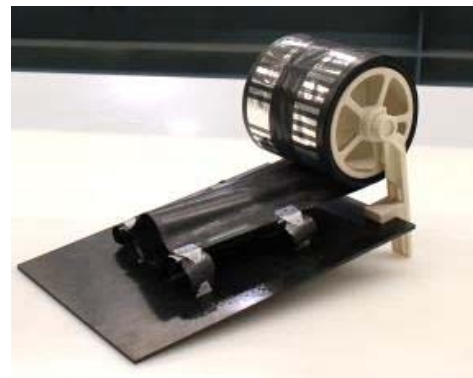
### 2.1 Boom Design

Arranged in a cross like configuration on the spacecraft the thin shell CFRP (carbon fiber reinforced plastics) booms feature a closed double  $\Omega$ -shaped cross section when deployed, also referred to as lenticular. It consists of two CFRP half shells that are symmetrically bonded along their flanges. These are made of a  $0^\circ/90^\circ$  one layer plain weave fabric with a wall thickness of 0.14 mm when cured. With a nominal height of 60 mm, a width of 74 mm and a total length of 4.3 m when deployed to each side of the of the spacecraft a specific boom mass of 32 g/m is achieved. Featuring two 8.6 m crossing booms in Gossamer-1, two boom sections of 4.3 m each are joined in the center of the boom-spacecraft-interface in order to achieve the intended dimensions. When flattened however, in stowed configuration, the boom has a nominal width of 108.25 mm as illustrated in Fig. 2 a). The material's elasticity and the omega shaped cross section of the half shells enable the booms to be flattened out over the whole length and to be rolled up on the cylindrical boom hub inside each deployment unit for stowage. Demonstrating this main feature Fig. 2 b) depicts a partially flattened and rolled up boom (functional model).

For simplification the tested booms however consist of the afore described boom of 4.3 m in length joined to a short boom piece of 130 mm in length resembling the opposing boom section. This is due to the fact that only one of the four boom ends of Gos-1 's boom cross is tested, profiting from its symmetry. The boom assembly itself is fixed with elastic hinges into the boom-spacecraft-interface, or fixed in a clamping device depending on the configuration tested.



a) Main dimensions in deployed and stowed condition



b) Boom stowed on a boom hub and fixed in its flexible interface (functional model)

Fig. 2: Gossamer-1 boom features

### 2.2 Interface Design

Two interfaces were used in the here described boom tests: An ideal interface (further described in section 3.3), clamping the boom root at its fully deployed cross section, and a realistic Boom-Spacecraft-Interface (BSI), that is explained in the following. Having its purpose in the fixation of the boom to the spacecraft, it is able to mimic the boom's cross sectional deformations that occur throughout the deployment process. The boom is adhesively bonded into the interface frame on four areas on both upper and lower sides of the boom flange with flexible hinges. Additionally it is bonded as well on two areas of its upper and lower convex side to guiding pins (further referred to as anvil). This fixation into the interface frame is illustrated in the images of Fig. 3 a) with the bonding areas marked red. For stowing/coiling up the boom onto the hub of the deployment unit, the boom is forced to be flattened out. Compared to the boom's full cross sectional dimensions, for stowage the cross sectional height near the coiled up region is reduced while the width is increased. This results in a cross sectional semi-state of the boom between fully deployed and flattened while fixed in the BSI, as depicted in Fig. 3 b). However, when the deployment begins the cross sectional dimensions of the fixed boom region change to the fully deployed shape, due to uncoiling the boom, and the interface needs to adapt. Realizing this crucial feature, the BSI makes stowage possible,

prevents the boom from being damaged and consequently enables to realize the method of boom tip deployment. This provides the full areal stiffness of the boom at the point of the largest bending loads, the fixation at the spacecraft. The flexible interface as used in the here presented boom tests, a fully functional model, is shown in Fig. 3 c). It consists of several CFRP parts that are adhesively bonded by flexible hinges and a base plate forming a collapsible frame structure. Providing a higher stiffness when deployed and making stowage possible, four CFRP tape springs are supporting this structure and deploy by the intrinsic stored energy once the booms are unrolled to the up-right (deployed) configuration (compare with Fig. 3).

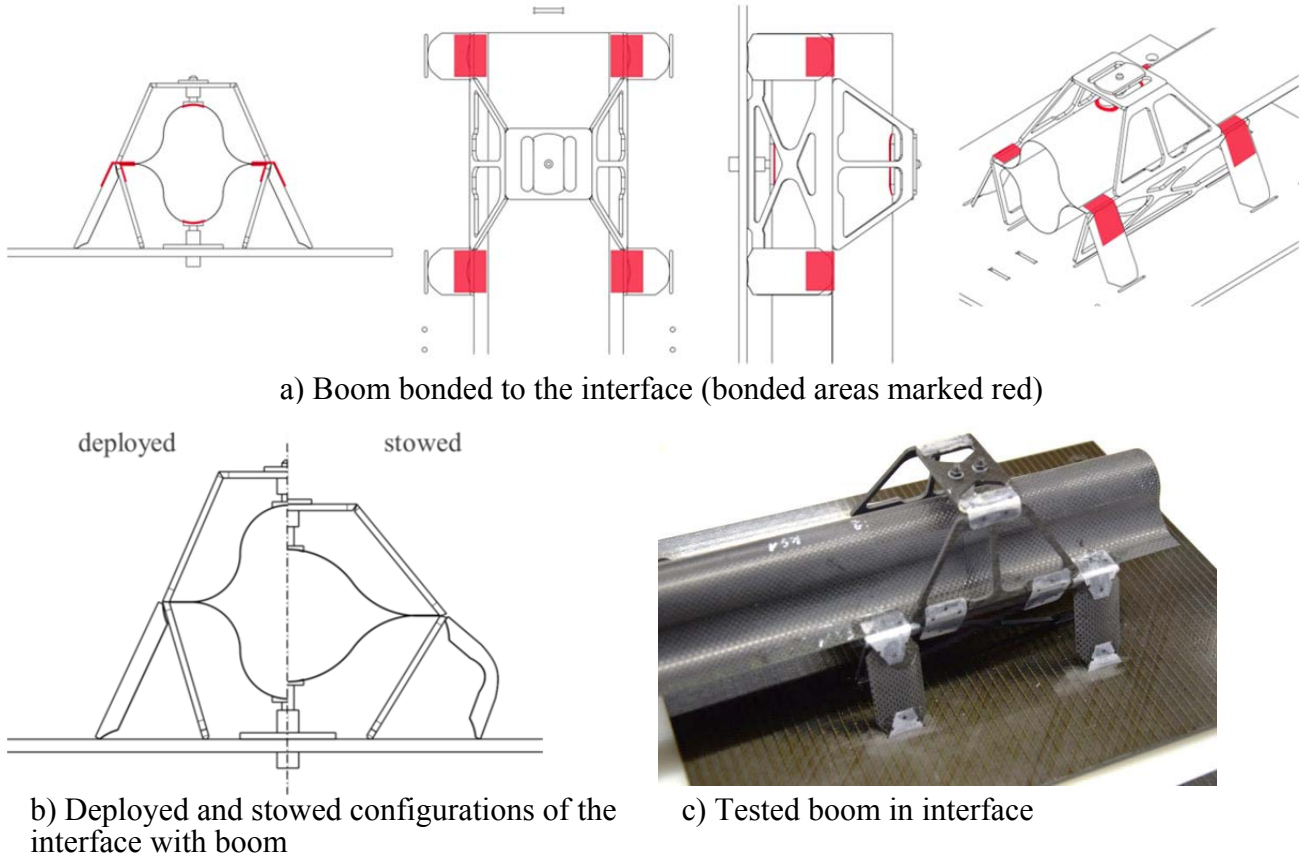


Fig. 3: Flexible Boom-Spacecraft-Interface of Gossamer-1

### 2.3 Main Loads on Booms

The main loads on the boom occur due to forces generated by tautening the sails, the solar wind, the residual atmosphere and acceleration forces introduced by structural masses (deployment units attached to boom tips) when in operation phase. During deployment, forces to unfold the sails and booms including their mechanisms have to be applied overcoming friction, pulling out wrinkles and pushing away the boom deployment units. This is resulting in a load vector, a combination of primary forces, for each sail segment corner acting on the connected booms tip, as illustrated in Fig. 4 a). Primary forces in-sail-plane, out-of-sail-plane and in axial boom direction are acting on the boom-sail subsystem as illustrated in Fig. 4 b) with  $F_y$ ,  $F_x$  and  $F_z$  respectively. Combining the primary loads resembles the resulting load vector that is applied by each corner of a sail segment to a boom tip. Further named  $F_s$ , standing for the sail force on a boom, this vector is oriented with an in-sail-plane angle of attack  $\alpha$  and an out-of-sail-plane angle of attack  $\beta$ , both measured between the boom flange and load path on the sail. In theory two sail corners adjacent to a boom tip apply a symmetrical pair of load vectors, leading to a symmetrical overall load introduction into the booms. Nevertheless in reality unsymmetrical loadings, as indicated with different size of load vectors in Fig. 4 a), will occur. Thus leading to a worst case scenario of only one load vector of a pair acting on the boom, resembling the case one sail is taut and the adjacent one slack.

Occurring main loads on the boom (see also Fig. 4 b) can be divided into:

- (1) Lateral force component in-plane (with respect to the flange plane of the boom)), here defined as  $F_x$ , leading to in-plane bending
- (2) Lateral force component out-of-plane (with respect to the flange plane of the boom), defined as  $F_y$ , leading to out-of-plane bending
- (3) Axial force component  $F_z$  (axial compression) leading to column buckling

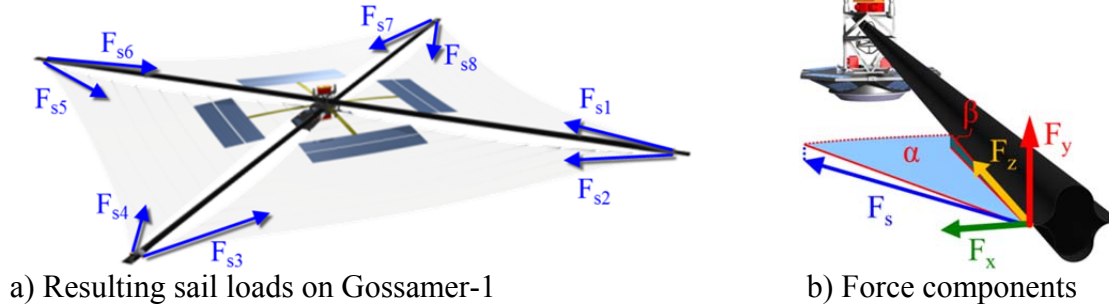


Fig. 4: Boom Loading

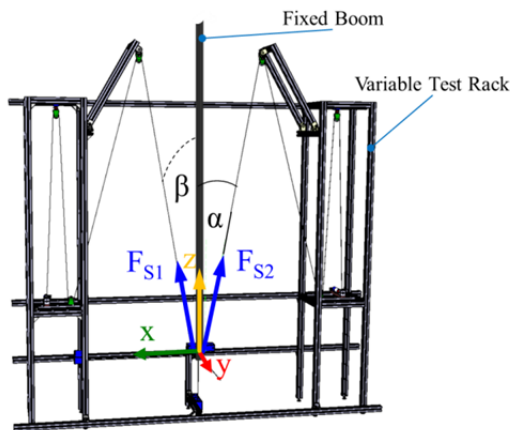
### 3. EXPERIMENTAL APPROACH

#### 3.1 Principle & Methodology

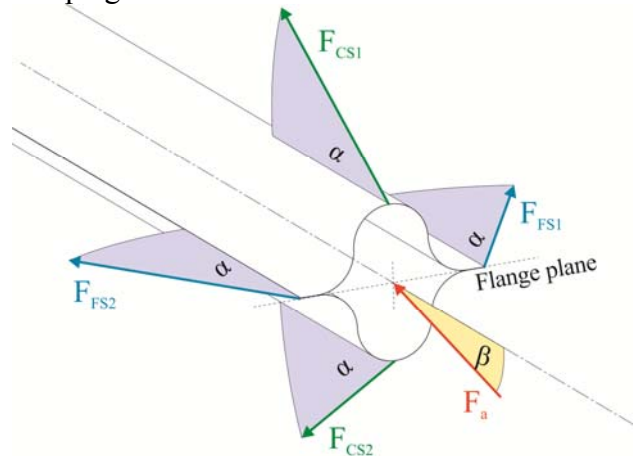
In the past mechanical characterizations of structural members of Gossamer spacecraft such as booms have been performed in different approaches. Many times they are conducted on specimen scale [4] or on full size scale e.g. in horizontal orientation with the necessity of using a complex gravity compensating device [5,6]. In order to reduce the influence of gravity leading to deformations of long structures in horizontal position due to their self-weight, another principle has been introduced, a vertical testing orientation [7,8]. This principle is applied in the here described tests with a vertical boom test stand serving the purpose to measure occurring forces and deflections of a boom when experiencing typical load cases. Furthermore this testing procedure has been previously performed on smaller boom types at DLR [9] and in preliminary tests of an early engineering model of Gossamer-1 in 2013 [2] as mentioned before.

In the vertical arrangement the boom is mounted hanging in the test stand, as depicted in Fig. 5. Being arranged in a symmetrical setup the boom is fixed in the center of the test stand and hanging with its tip pointing downwards. The methodology of testing aims to apply a load under a certain angle of attack at the boom tip while measuring the tip deflection and the applied forces. To realize this, a string (two strings depending on test configuration) attached at the boom tip is reeled up using a string-pulley-system with two electrical motors. This actuation is controlled by step positioning the motor rotation. The in-plane angle of attack  $\alpha$ , between strings and boom axis, is set to the according angle with a variable pulley system and load rack. For lateral bending only the in-plane angle  $\alpha$  is adjusted while for axial compression a superimposed out-of-plane angle  $\beta$ , resembling a realistic geometric relation between Gossamer-1's boom tip plane and sail fixation point on the spacecraft. Considering these angles as starting point this is seen as simplification due to the changes over a test run with changing geometric relations between boom tip, strings and load rack with increasing boom tip deflections. Reeling up a string (two strings, depending on test configuration) results in a boom tip deflection and in the string forces  $F_{S1}$  and  $F_{S2}$ , within the x-y-plane of the test stand (see Fig. 5). Measuring the boom tip deflections in all 6 degrees of freedom a photogrammetry system is used while only the translational deflections are of interest within this test campaign. The occurring string forces, resembling the sail forces in sailcraft, are measured using two force sensors integrated in a pulley system. Acquiring sensor data was achieved by a synchronous measuring process realized by triggering all sensing systems at a rate of 9 Hz and a pull-in-speed of the load applying string of 200 mm/min. This provides data points with identical timestamps for data convergence and analysis and is realized for all performed test runs. Extending the configuration found on Gossamer-1 to gain additional knowledge for future

applications using the booms in a rotated orientation; both convex and both flange sides of the boom are tested and mechanically characterized under several values for  $\alpha$ . Asymmetrical conditions as found in a worst case scenario for Gossamer-1, simulated by lateral bending, only one boom side is loaded at a time by deflecting the boom tip. Applying this on each side results in the four lateral forces:  $F_{CS1}$  and  $F_{CS2}$ , on the convex sides, and  $F_{FS1}$  and  $F_{FS2}$ , on the flange sides. To acquire an axial load case a symmetrical load introduction by pulling simultaneously on two opposite boom sides is realized, under the additional out-of-plane angle  $\beta$ . This results in the axial compressive force  $F_a$  under the geometric offset between boom tip and sail fixation on the spacecraft. The resulting and measured forces for each load case are illustrated in Fig. 5. Although important for a complete mechanical boom characterization, torsional flexural buckling behavior has not been investigated in the here described test campaign.



a) Simulated sail loads ( $F_{S1}$ ,  $F_{S2}$ ) applied on the boom fixed in the test stand



b) Applied lateral and axial loads on booms

Fig. 5: Loads applied in test stand

### 3.2 Test Stand & Setup

Reaching over 3 floors of the building the test stand, located at the DLR Space Structures Lab @ Uni of DLR Braunschweig, provides an adjustable boom test length from 1.5 to 13 m, using a height variable mounting table in a guide frame where the boom root is mounted on. As depicting the main testing system (guide frame not displayed) in Fig. 6 it consists of the following elements: The Sensor & Load Rack, hosting the force sensors, pulleys and actuators (motors), being adjustable to realize angles of attack  $\alpha$  from  $0^\circ$  to  $90^\circ$  for in-x-z-plane and  $\beta$  from  $0^\circ$  to  $10^\circ$  perpendicular to the x-z-plane (compare with test stand axis in Fig. 5 a); the A/D Converter & DAQ System gathering the measured force values; a computer with a developed test software in LabVIEW© environment that controls the actuators and processes data from the DAQ system; the Photogrammetry system (System: MoveInspect© HR, by AICON) with two 5 megapixel cameras and a separate computer with a specific on board 3D-Measuring software that is receiving the trigger signal from the LabVIEW Computer. Furthermore the boom tip is equipped with a Visual/Load Adapter, providing retroreflective targets for photogrammetry measurements as well as for load introduction.

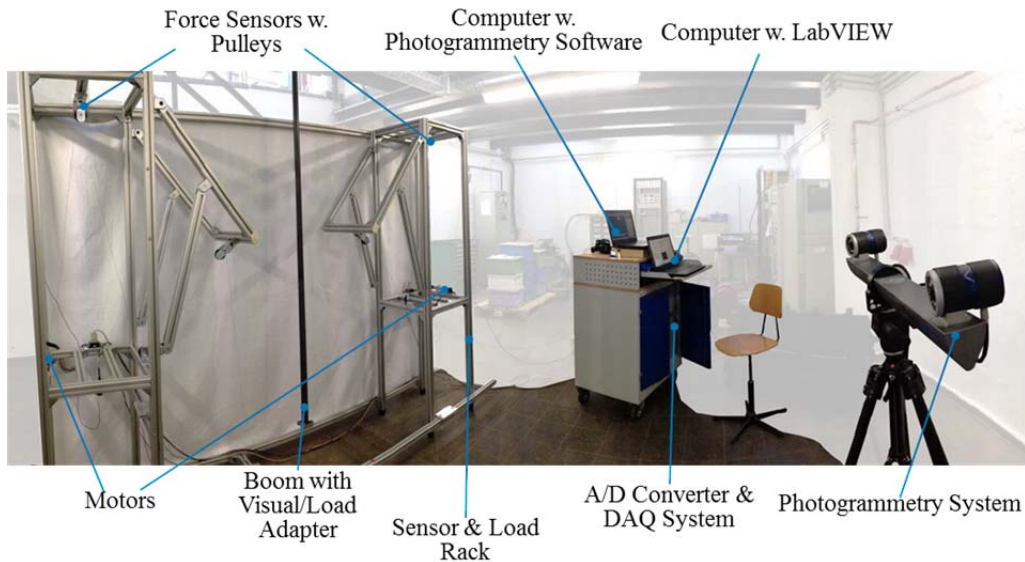
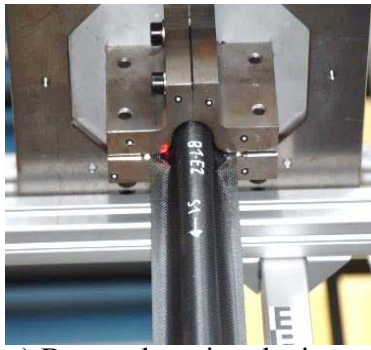


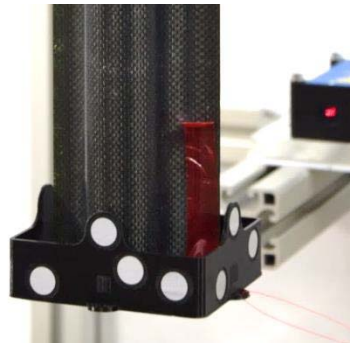
Fig. 6: Boom test stand & setup

### 3.3 Load Application & Boundary Conditions

While the boom in all tests is mounted vertically in the test stand, the fixation of the boom root is different for the test configuration with the ideal interface than it is for the one with the realistic Gossamer-1 interface. For the ideal interface a massive metal clamping device is used (see Fig. 7 a), consisting of four brackets that are tightened around a metal core inside the test specimen and bolted to a metal plate, thus inhibiting all degrees of freedom at full cross sectional dimensions on a length of 100 mm. The realistic interface however is providing flexibility to some degree as described in section 2.2. although it is tested in the deployed configuration (see Fig. 3) with the full cross sectional size of the boom. Hanging upside down the boom tip on the other hand is able to realize translation and rotation in all 6 degrees of freedom, while the load is introduced into the tip by different Visual/Load Adapters that inhibit cross sectional deformations. In the ideal configuration the used Visual/Load Adapters (Fig. 7 b and c) provide the cross sectional dimensions of a fully deployed boom, thus enabling a constant and maximum second moment of area throughout the complete boom length. In contrast to this the Visual/Load Adapters for the realistic Gossamer-1 configuration provide a semi state of cross sectional dimensions between fully flattened and deployed. Simulating the real boom-sail-interface at the boom tip in this way, a decreasing second moment of area starting from the boom root is provided. Additionally axial fixation of the Visual/Load Adapters here is provided by two bolts latched into a hole in the boom flange on each of the boom (see detail in Fig. 8 b). For lateral bending an asymmetric load introduction is realized under varying angles of attack of  $\alpha=22.5^\circ$  and  $45^\circ$  for the flange side direction; and  $\alpha=15^\circ$  and  $45^\circ$  for the convex side direction resulting in the forces  $F_{FS1}$ ,  $F_{FS2}$  and  $F_{CS1}$ ,  $F_{CS2}$  respectively (compare to Fig. 5 b). These angles of attack derive from an idealized angle of the force vector acting on the deployed sail segment for a use case ( $22.5^\circ$ ) and two possible worst case scenarios ( $15^\circ$ ,  $45^\circ$ ). For lateral loading the load applying string is attached to only one side of the Visual/Load Adapter at a time, as shown in Fig. 7 b). Load application for axial compression is realized with a symmetrical load introduction and an in-plane angle of attack of  $\alpha= 2^\circ$  from two opposite sides, while superimposing an out-of-plane angle of attack of  $\beta= 3^\circ$ , resulting in  $F_a$  (compare to Fig. 5 b). As depicted in Fig. 7 c) and Fig. 8 c) for each configuration type, the Visual/Load Adapter is equipped with a pulley guiding the load applying string and transforming the applied string forces into an axial load. The pulley also helps to balance load differences applied by the two motors.



a) Boom clamping device

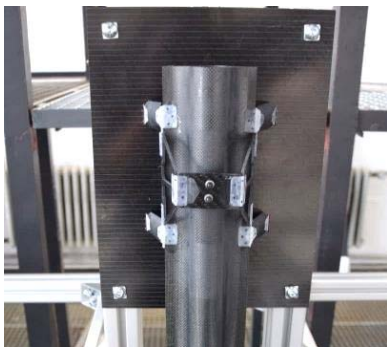


b) Visual/Load adapter for later bending



c) Visual/Load adapter with pulley for axial compression loading

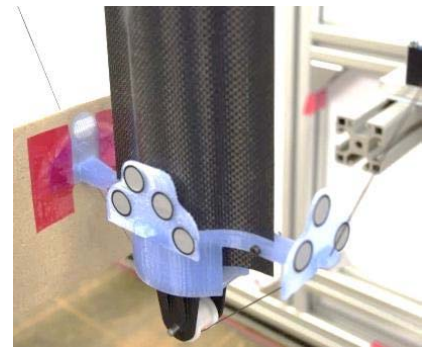
Fig. 7: Ideal boom root fixation and load application adapters



a) Boom in flexible interface



b) Visual/Load adapter for later bending



c) Visual/Load adapter with pulley for axial compression loading

Fig. 8: Realistic boom root fixation and load application adapters

## 4. RESULTS & DISCUSSION

A total number of 6 booms have been tested, 3 in the ideal interface and 3 in the realistic interface. Due to the effort of manufacturing and to generate as much data as possible each boom has been tested in different load configurations. From mechanics and previous boom tests it is known that buckling due to lateral bending is likely to occur near the fixed boom end [2]. This gives the opportunity to test both ends of each boom. Furthermore testing each boom end in both flange sides and both convex sides is possible based on the effect that for lateral bending the compressive loaded side might experience damage while the elongated side does not. In the configuration of axial compression however, only one boom end is tested, since in most cases Euler buckling is observed resulting in buckling (snapping in) at the boom's mid-section.

In the following sections the results of all tested booms in ideal and realistic interfaces, under lateral bending and axial compression are described. Differences in results between the interfaces as well as between the different boom sides are compared and discussed.

### 4.1 Lateral Bending Tests

Results of the tested booms loaded at the flange side comparing both ideal (clamped) and realistic (flexible) interface configurations are summarized in Table 4-1, while Table 4-2 compares the results of the tested convex sides of both configurations.

Both tables display the boom number, the angle of attack  $\alpha$ , the run number, the critical buckling force  $F_{\text{scrit}}$  at which a boom fails due to buckling (snap-in), the relation giving the percentage of  $F_{\text{scrit}}$  compared to the first test run, considered to be without damages prior to buckling, for each series, and the boom tip deflection  $s_x$  at which the boom fatally buckled. Additionally a failure characteristic is given for the results on the convex side of the tested flexible interface. This

indicates an unexpected failure other than buckling e.g. failure of interface components. For a better comparison all values are expressed in positive numbers and are therefore not indicating the direction of boom tip deflection within the test stand coordinate system. Each combination of tested boom, angle of attack and boom side (test scenario) comprises of 3 subsequent test runs. When looking at the results of the convex sides for the flexible interface in Table 4-2, only values for one of the two sides is given. Here only one convex side could be tested due to the lack of clearance between the interface-plate and the deflecting boom of the used engineering model.

Table 4-1: Lateral Bending – Flange Sides

Boom No.	FS1 & FS2 (averaged)				
	Ideal Interface		Flexible Interface		
Angle of attack $\alpha$ [°]	Run No.	$F_{scrit}$ [N]	Relation [%]	$s_x$ [mm]	at $F_{scrit}$
B1	15	1	5.4	100.0	170.2
		2	4.2	78.3	154.3
		3	4.1	76.4	147.2
B2	45	1	2.6	100.0	145.9
		2	2.4	91.2	130.1
		3	2.4	89.5	144.2
B3	90	1	3.2	100.0	181.0
		2	3.1	97.1	171.2
		3	3.0	94.5	163.7

Table 4-2: Lateral Bending – Convex Sides

Boom No.	CS1 & CS2 (averaged)					Failure characteristic
	Ideal Interface		Flexible Interface			
Angle of attack $\alpha$ [°]	Run No.	$F_{scrit}$ [N]	Relation [%]	$s_x$ [mm]	at $F_{scrit}$	
B1	15	1	8.8	100.0	207.9	Anvil
		2	7.1	80.4	172.7	
		3	6.9	78.5	168.5	
B2	45	1	3.5	100.0	202.8	Anvil
		2	3.3	93.9	189.7	
		3	3.0	86.2	174.5	
B3	90	1	2.4	100.0	178.5	Anvil
		2	2.0	81.5	169.9	
		3	2.0	81.1	171.4	

In general the results for the flange sides of both configurations in Table 4-1 show that with smaller angles of attack, higher values of the critical buckling force  $F_{scrit}$  are reached (except for B3 at 90°, compared to B2 at 45°), while this effect is not consistent for the maximum deflections  $s_x$ . It is also evident that reached critical buckling forces  $F_{scrit}$  for the first test run of a test scenario is the maximum; subsequent test runs show decreased values. This is also the case for the according deflection values and in compliance with the assumption that damages caused by the first test run are reducing values of subsequent test runs and load capability to some degree. The test scenario with the smallest loss in load capability is the ideal configuration under  $\alpha=90^\circ$  with the 1<sup>st</sup> test run of  $F_{scrit}=3.2$  N, the 2<sup>nd</sup> test run with  $F_{scrit}=3.1$  N reaching 97.1 % and after the 3<sup>rd</sup> test run  $F_{scrit}=3.0$  N still achieving 94.5 % of the initial value. On the other hand the test scenario with the largest loss in load capability is the ideal configuration under  $\alpha=15^\circ$  with the 1<sup>st</sup> test run having  $F_{scrit}=5.4$  N, the 2<sup>nd</sup> test run with  $F_{scrit}=4.2$  N reaching 78.3 % and after the 3<sup>rd</sup> test run  $F_{scrit}=4.1$  N still achieving 76.4 % of the initial value.

Results of the convex sides of both configurations in Table 4-2 are again indicating that in general a smaller angle of attack leads to a larger critical buckling force  $F_{scrit}$ , while at the same time larger boom tip deflections  $s_x$  are reached. This is obvious for the ideal configuration. Here a loss in load carrying capability over subsequent test runs is visible, reaching 78.5 % of the initial buckling force value at  $\alpha=15^\circ$  after the 3<sup>rd</sup> test run, resembling the largest loss; and still achieving 86.2 % of the initial buckling force value at  $\alpha=45^\circ$  after the 3<sup>rd</sup> test run of the initial value, resembling the smallest loss. For the flexible configuration a loss in load carrying capability is not consistent over the performed test runs. Instead a significant increase in buckling force  $F_{scrit}$  can be observed for the 3<sup>rd</sup> test run under  $\alpha=22.5^\circ$  achieving  $F_{scrit}=10.7$  N, resembling an increase to up to 230.4 %, and for the 2<sup>nd</sup> test run at  $\alpha=45^\circ$  achieving  $F_{scrit}=9.7$  N, resembling an increase to up to 288.1 %, compared to the according 1<sup>st</sup> test runs. This can be explained by different occurring failure phenomena on boom and interface observed. A failure at a connection point of the interface occurred at the bonded aluminum anvil that distributes axial loads from the convex boom sides into the surrounding interface structure (see also Fig. 3), thus not reaching the much higher buckling load of the boom itself. After repairing the anvil-boom connection in a sufficient manner, values for buckling failure were much higher for subsequent test runs. Assuming its reason in insufficient adhesive quality, the

bonding was renewed after each failure and the next test run was performed. In the following test runs with a sufficient bonding the boom failed due to local buckling, resulting in a more than doubled value. In the test scenario of boom B6 in the flexible interface, under  $\alpha = 90^\circ$ , failure occurred in all three test runs due to the breaking bonding of the anvil, resulting in comparably low load values. For scenarios testing the flange sides, such phenomenon could not be observed. Common buckling patterns and failure characteristics of the failing booms are depicted in Fig. 9, applying for both interface types. Additionally Fig. 10 displays boom failure and buckling patterns with respect to the different interfaces. When comparing critical buckling force values  $F_{crit}$  of both configurations that were reached at the convex side for similar test scenarios, the flexible interface (realistic configuration) achieved the highest as well as the lowest values.

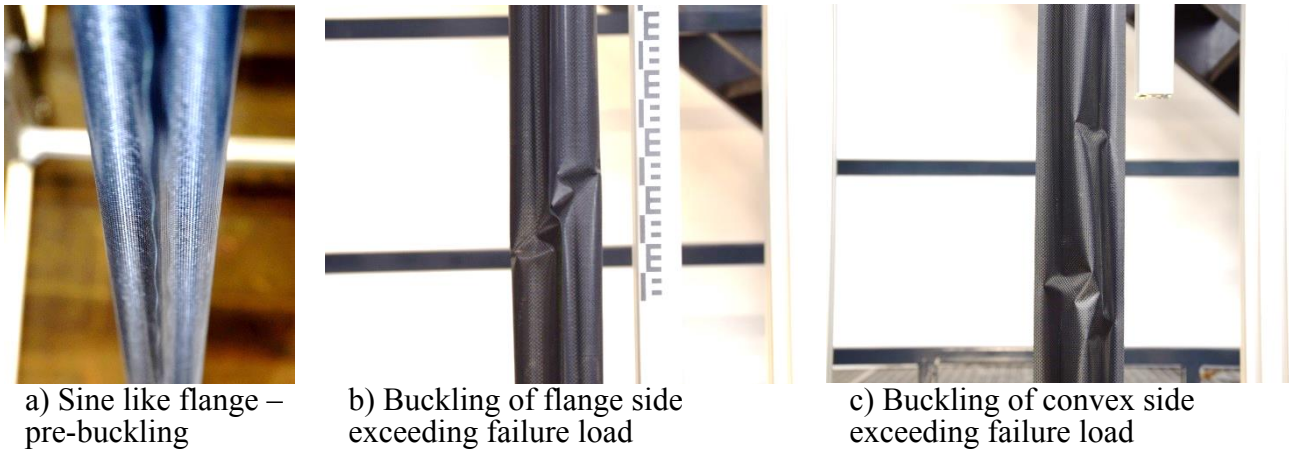


Fig. 9: Common buckling patterns on the tested booms under lateral bending

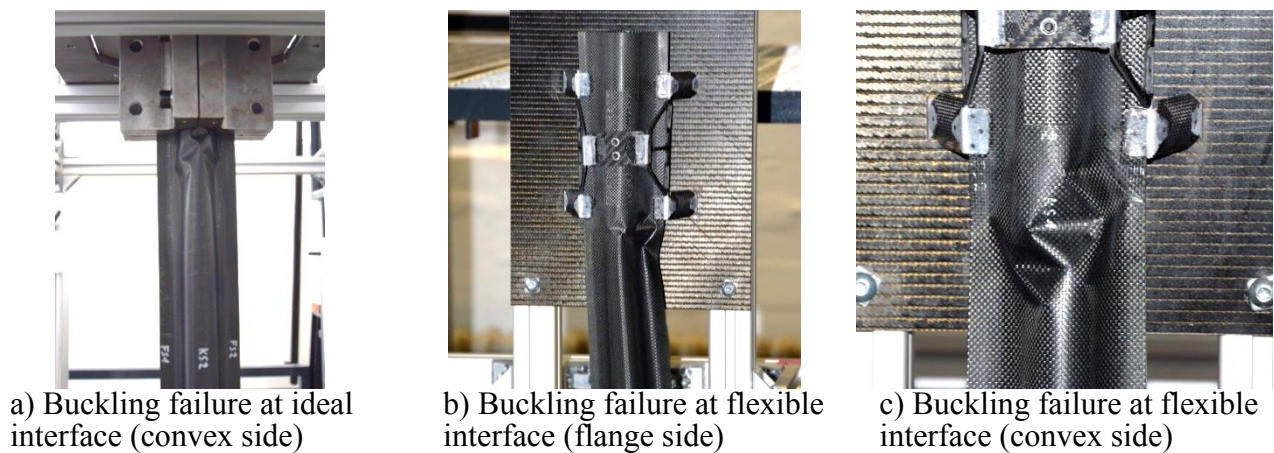


Fig. 10: Buckling failure at the interfaces

Decreasing values for the critical buckling force  $F_{crit}$ , resembling a reduction of load carrying capability, for subsequent test runs can be explained with occurring damages in the boom's CFRP shells and bond lines of the flanges when overloading the boom. Damages like cracks and delamination, visible and invisible, lead to this effect, as one would expect. Higher load values of  $F_{crit}$  at smaller angles of attack compared to larger angles have their origin in a higher portion of the favorable axial loading for such structures, thus leading to higher load carrying capability. A difference in remaining load carrying capability after several subsequent test runs between convex and flange sides or ideal and flexible configuration cannot clearly be distinguished. However the boom tip deflections  $s_x$  at the event of failure are higher for all test scenarios on the flange sides in flexible configuration compared to the ideal configuration, due to the flexibility of its interface. When comparing the results of the convex and flange sides in the clamped configuration for  $\alpha = 15^\circ$  and  $45^\circ$  the convex side can carry higher loads at larger boom tip deflection  $s_x$ . For  $\alpha = 90^\circ$  however

the flange sides can carry higher loads at a similar level of  $s_x$ . This is at least partially in contradiction to the theoretic second moments of area of the boom with  $I_x = 8977 \text{ mm}^4$ , in convex side direction, being smaller than  $I_y = 11710 \text{ mm}^4$ , in flange side direction. Knowing this fact the flange side could be expected to carry higher loads. However, the lower loads for the flange side can be explained with the resulting pre-buckling patterns, exhibiting sine wave like buckles along a loaded flange (see Fig. 9 a). This seems to have a negative and load capability reducing effect, as observed already in previous boom tests [2]. When looking at the maximum values of all test runs of the critical buckling force  $F_{\text{scrit}}$ , the flexible interface achieves higher values than the ideal configuration, for the convex sides. For the tested flange sides no significant difference or general bias towards one configuration, regarding the critical buckling force, can be observed. The boom tip deflections  $s_x$  on the other hand are in general higher for the flexible configuration than for the ideal configuration, for all tested scenarios, having its origin in the beneficial flexibility of the realistic interface when giving in and releasing local tension to surrounding boom shell areas that are free to deform. Comparing past test results from [2] for booms tested under  $45^\circ$ , at their flange sides, in the flexible interface, higher maximum values for  $F_{\text{scrit}}$  and  $s_x$  are achieved in the tests presented here. This is expected to have its reason in the matured interface design. On the other hand the acquired test results are still off of FEA results [2] for a maximum  $F_{\text{scrit}}$  by about 16 %.

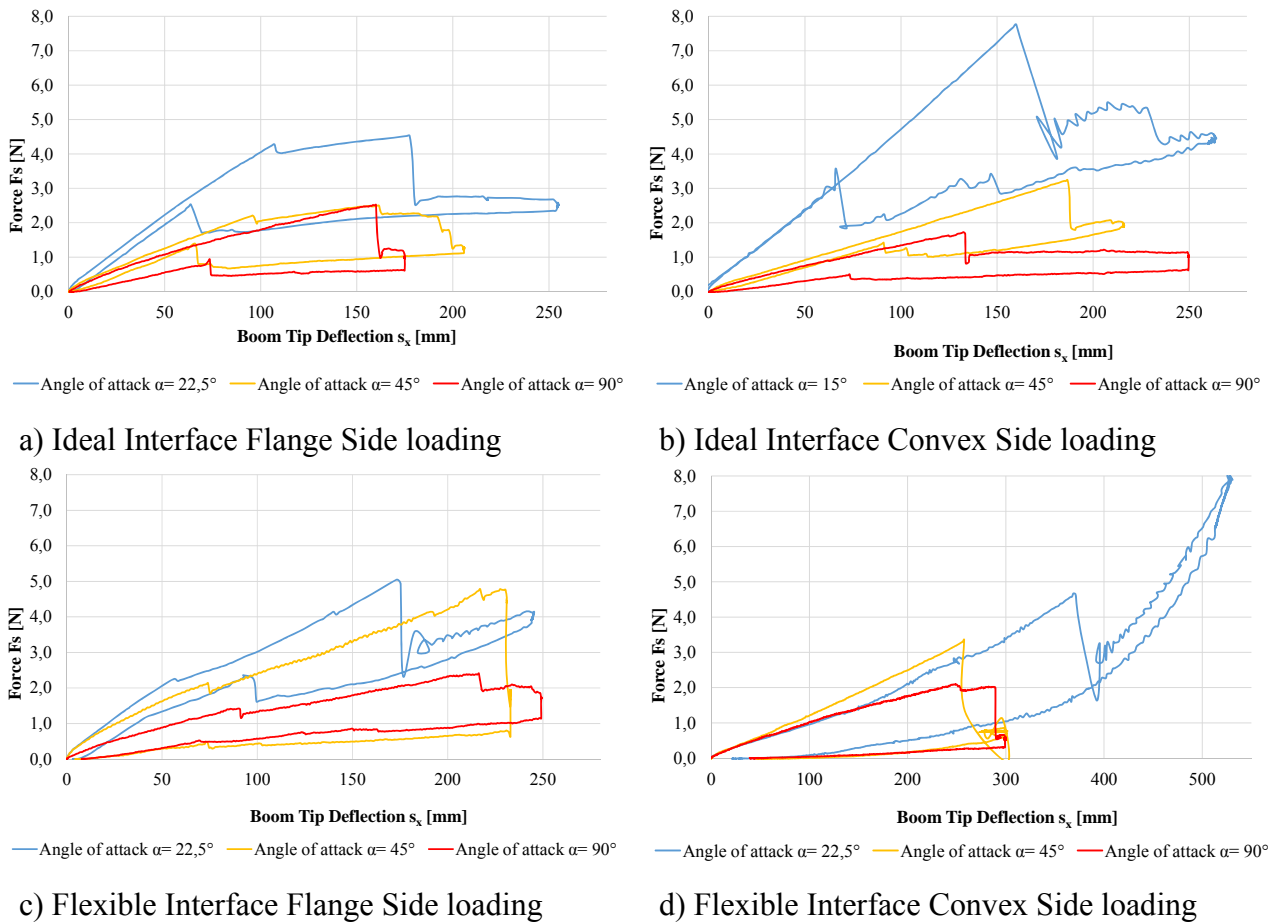


Fig. 11: Exemplary result graphs for lateral bending in ideal and flexible interface and under different angles of attack

Furthermore typical load deflection curves showing the applied force  $F_s$  versus the boom tip deflection  $s_x$  for each interface type and loaded boom side, under different angles of attack, were acquired as depicted in Fig. 11.

The course of test and mechanical behaviour of the boom can generally be explained in both images of Fig. 11. Starting with an almost linear behaviour with increasing force and deflection, the typical curves show sudden load drops, indicating the failure and snap-in of the boom. In Fig. 11 a) for

example, the linear course is interrupted by a small uncritical load drop continuing with a smaller slope until buckling failure. After fatal buckling, deflection is continuing (further pulling the string) with an oscillating force value, caused by the swinging boom after the rapid load drop, until the motor is stopped. The rotation of the motor is now reversed and string is given, leading to a reduction in boom tip deflection while the boom is gaining its initial shape. After a certain reduction in boom tip deflection is reached the boom snaps back (unbuckles) and the load deflection curve returns to an almost linear behaviour. The motor is still in reverse mode driving back to its starting position as it is step controlled, while the boom tip deflection is reduced to its initial value. When comparing the two parallel linear sections of a curve a hysteresis shown as offset on the vertical coordinate axis is clearly visible. This behaviour is stronger developed in the behaviour of the flexible interface. It arises due to setting processes of the tape springs, anvil and elastic joints of the flexible interface and is also apparent in the residual deflection value when the boom is completely released.

When testing the flange side, the boom experiences a sine like buckling wave pattern along the flanges as shown Fig. 9 a) prior to fatal buckling. This sine like wave triggers small uncritical buckles on the convex sides of the boom showing in a small load drops that do lead to a snap-in right away. Once a certain load and boom tip deflection is reached the sine wave like buckles transform into a larger single buckle at the flange, indicating the collapse of the flange under compressive loads. For the flexible interface more than one uncritical small load drop occurs before finally snapping in. This can be explained by arising small buckles on the boom shell and additional yielding of the tape springs of the flexible interface. In contrast to this a load deflection curve of the convex side does not show an intermediate load drop, instead the linear section continues undisturbed until the fatal load drop. In the graph of Fig. 11 d), at  $\alpha = 22.5^\circ$ , a behaviour introduced by the testing procedure itself shows an increase in boom tip deflection and applied force after the fatal buckling event has occurred. This is due to the continuation of the motor that winds up the load applying string. The recurrent increase of  $F_s$  arises due to a stabilizing effect of the buckling pattern of the damaged boom. Nevertheless at this point the boom is strongly buckled and damaged, and the tip deflection has a value above an acceptable level for a structure like a solar sail, thus leaving the last values directly before the sudden load drop as maximum critical buckling force  $F_{scrit}$ . Again it becomes obvious that smaller angles of attack lead to a higher maximum critical buckling force  $F_{scrit}$ .

## 4.2 Axial Compression Tests

The axial compression test was performed on three booms in ideal and three in flexible configuration. All acquired test results are summarized in Table 4-3 and Table 4-4 giving the following values: Boom number, in-plane angle of attack  $\alpha$ , out-of-plane angle of attack  $\beta$ , number of test run, the critical buckling force at which a boom fails due to buckling measured by the left sensor with  $F_{scritLeftside}$  side and with  $F_{scritRightside}$  for the force sensor on the right side, the average force value of both sensors  $F_{scritAverage}$ , and the resulting force vector in axial direction  $F_{a,res}$ . The purpose was to determine the maximum bearable axial load of the boom at which fatal buckling (destruction/damaging) occurs. In the tested configuration the load was applied by one string guided through the eyelets of the flange sides of the Visual/Load Adapter over a pulley that was fixed to the adapter as explained in section 3.3.

For a better comparison of both configurations, using different angles of attack, the axial load component vector is used and calculated as described in Eq. 1.

$$F_{a,res} = (F_{scritLeft\ side} + F_{scritRight\ side}) \times \cos \alpha \times \cos \beta \quad (1)$$

The intended symmetrical load under the in-plane angle of attack of  $\alpha$  to each side, self-stabilizing its centre position using the free pulley, could be achieved for the ideal interface configuration on an acceptable level and fairly well for the flexible interface configuration. This is can be observed

when comparing the measured load values  $F_{\text{scrit}}$  of the right and left force sensors in Table 4-3 and Table 4-4. Differences in friction from guiding eyelets of the Visual/Load Adapter, possible tilting of the Visual/Load Adapter on the boom tip or possible undesired curvature of the boom are assumed to be the reason for this. When analyzing the results subsequent test runs could only be performed for the flexible configuration. In the test runs with the ideal interface fatal and destructive buckling as illustrated in Fig. 12 a) and b) occurred, making another test run impossible. Furthermore the averaged load values  $F_{\text{scritAverage}}$ , are of very similar size throughout all tested booms (comparing the according 1<sup>st</sup> test runs). For the ideal interface the maximum deviation is lower than 10 %, for the flexible interface about 12 %, indicating an acceptable repeatability. However, the differences also show that small imperfections due to manual manufacturing can have an influence on the test results, assuming the test stand and test procedure providing a consistent quality. Comparing the results of the two interface configurations, in specific the averaged failure loads  $F_{\text{scritAverage}}$  (load on actuation strings of each side, averaged) and the axial load component  $F_{a,\text{res}}$ , the ideal interface achieves more than three times the values of what the flexible configuration can achieve. Having its reason in different failure modes the booms in ideal configuration buckle globally almost in the middle of the boom length as depicted in Fig. 12 a), while the booms in the flexible interface fail close to the load introducing Visual/Load Adapter, that additionally constricts the booms cross section, as shown in Fig. 12 c). This demonstrates that not only the interface at the boom fixation point but also the load introducing adapters have a large impact on achievable buckling loads.

Table 4-3: Axial Compression – Ideal interface

				Flange Sides FS			
Boom No.	in-plane Angle of attack $\alpha$ [°]	out-of-plane Angle of attack $\beta$ [°]	Run No.	$F_{\text{scrit Left side}}$ [N]	$F_{\text{scrit Right side}}$ [N]	$F_{\text{scrit Average}}$ [N]	$F_{a,\text{res}}$ [N]
B1	3	0	1	111.16	131.19	121.18	242.02
B2	3	0	1	117.74	138.59	128.17	255.98
B1	3	0	1	121.60	136.20	128.90	257.45

Table 4-4: Axial Compression – Flexible Interface

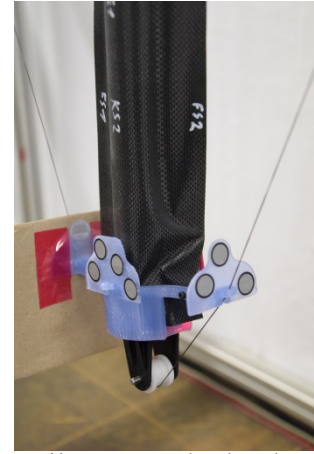
				Flange Sides FS				
Boom No.	in-plane Angle of attack $\alpha$ [°]	out-of-plane Angle of attack $\beta$ [°]	Run No.	$F_{\text{scrit Left side}}$ [N]	$F_{\text{scrit Right side}}$ [N]	$F_{\text{scrit Average}}$ [N]	$F_{a,\text{res}}$ [N]	R [%]
B4	22.5	3	1	37.72	36.11	36.91	68.11	100.0
			2	22.63	22.78	22.71	41.90	61.5
			3	19.78	21.43	20.61	38.02	55.8
			4	16.88	17.62	17.25	31.83	46.7
B5	22.5	3	1	32.93	32.81	32.87	60.66	100.0
			2	27.89	27.90	27.89	51.47	84.9
			3	27.87	27.91	27.89	51.46	84.8
			4	27.51	27.52	27.51	50.77	83.7
B6	22.5	3	1	36.14	35.16	35.65	65.79	100.0
			2	31.66	30.75	31.20	57.57	87.5
			3	31.84	31.00	31.42	57.98	88.1
			4	31.60	33.00	32.30	59.60	90.6



a) Buckling under compression



b) Column buckling and destruction under axial compression



c) Failure near the load introduction at the Visual-Load-Adapter

Fig. 12: Buckling failure under axial compression

## 5. CONCLUSION

The investigation in this paper described the test setup, procedure and results of tested Gossamer-1 booms in its realistic interface, compared to an ideal one. Furthermore the design, functionality and setup of the boom and interface hardware as well as the vertical test stand were described.

A total number of 6 booms were tested in lateral bending loading and axial compression, in both ideal and realistic interface. Test results show that the smallest remaining load carrying capability throughout all test runs exceeded at least 65 % after the third subsequent test run, proving some robustness of the structural system. The results indicate that in general smaller angles of attack provide larger buckling loads, inherent by the favorable larger portion of axial loading for such boom structures. For lateral bending in both boom sides ideal and flexible interface configurations provide maximum buckling loads in the same order, while the flexible interface provides larger boom tip deflections. Booms tested under axial compression and in the ideal interface achieved at least three times higher buckling loads than in the flexible interface. Such a distinguished statement is not possible for lateral bending. In contrast to theory, regarding the second moments of area, e.g. the flange sides of a boom tested under  $\alpha = 90^\circ$  can carry higher loads at a similar levels of  $s_x$ . This is based on the typical sine like pre-buckling deformation of the flanges, as already acknowledged in [2]. As this and other examples show, different failure mechanisms lead to different values for buckling failure. For future investigations the here described tests show that a higher number of booms tested are necessary to give a reliable failure prediction with statistical reliability. Furthermore computational models should be adjusted to incorporate all occurring effects.

## 6. ACKNOWLEDGEMENTS

The authors would like to thank the European Space Agency (ESA) and the German Aerospace Center (DLR) for funding this investigation within the framework of the co-sponsored Networking/Partnering Initiative (NPI): "Robust and Tolerant Gossamer Structures", NPI Proposal Reference Number: 193-2011.

## 7. REFERENCES

- [1] U.R.M.E. Geppert, B. Biering, F. Lura, J. Block, M. Straubel, R. Reinhard, The 3-step DLR–ESA Gossamer road to solar sailing, *Advances in Space Research* 48 (2011) 1695–1701.
- [2] M. Straubel, M.E. Zander, C. Hühne, Design and Sizing of the GOSSAMER Boom Deployment Concept *Part III Technology Activities: Part III Technology Activities*, in: M. Macdonald (Ed.), *Advances in Solar Sailing*, Springer-Verlag, 2014, pp. 593–608.
- [3] M. Hillebrandt, S. Meyer, M.E. Zander, C. Hühne, M. Sinapius, Deployment Testing of the De-Orbit Sail Flight Hardware.
- [4] J.A. Banik, T.W. Murphey (Eds.), Performance Validation of the Triangular Rollable and Collapsible Mast, Utah State University, 2010.
- [5] T. Mann, V. Behun, D. Lichodziejewski, W.C. Derbes, D. Sleight, GROUND TESTING A 20-METER INFLATION DEPLOYED SOLAR SAIL, in: *47th AIAA/ASME/ASCE/AHS/ASC Structures, Structural Dynamics, and Materials Conference*, 2006.
- [6] D. Lichodziejewski, W.C. Derbes, W.K. Belvin, K. Slade, T. Mann (Eds.), DEVELOPMENT AND GROUND TESTING OF A COMPACTLY STOWED SCALABLE INFLATABLY DEPLOYED SOLAR SAIL, AIAA, 2004.
- [7] J.D. Hinkle, L.D. Peterson, P. Warren (Eds.), Structural Performance of an Elastically Stowable Tubular Truss Column, AIAA, 2002.
- [8] E.L. Pollard, T.W. Murphey, G.E. Sanford, Experimental and Numerical Analysis of a DECSMAR Structure’s Deployment and Deployed Performance, in: *48th AIAA/ASME/ASCE/AHS/ASC Structures, Structural Dynamics, and Materials Conference*, Honolulu, Hawaii, 2007.
- [9] M.E. Zander, M. Hillebrandt, M. Sinapius, C. Hühne, MECHANICAL CHARACTERIZATION OF DEPLOYABLE THIN SHELL CFRP BOOMS FOR THE CUBESAT “DE-ORBIT SAIL”, in: *IAC 2015 – The 66th International Astronautical Congress*, Jerusalem, Israel, 2015.